

Field emission site density studies of amorphous carbon films

M.T. Kuo^{a,*}, P.W. May^b, M.N.R. Ashfold^b

^aMaterials Research Laboratories, Industrial Technology Research Institute, Building 77, 195 Chung Hsing Road, Section 4, Hsinchu 31040, Taiwan

^bSchool of Chemistry, University of Bristol, Cantock's Close, Bristol, BS8 ITS, UK

Received 19 November 2001; received in revised form 16 January 2002; accepted 31 January 2002

Abstract

Amorphous carbon (a-C) films have been deposited by radio frequency (RF) plasma chemical vapor deposition (CVD) using CH₄ gas mixtures at a DC bias of –300 V, and their field emission characteristics investigated, particularly with regard to the turn on/off behavior of emission sites. A phosphor-coated indium tin oxide (ITO) anode in a parallel-plate configuration was used for observing and characterizing the field emission sites. The field emission properties of a-C films annealed at 200 °C in vacuum for 48 h were also studied. Both the as-deposited and annealed films exhibit an exponential relationship between the emission current and the number of emissive spots on the phosphor screen (i.e. emission sites on the film). A new term, ‘emission site conductance’, the average emission current per site, in units of nA site⁻¹, is introduced to characterize the emission characteristics of an individual site. Thermal annealing of a-C films is shown to enhance both the density and the uniformity of emission sites, thereby reducing the current load per site. Such benefits are most likely attributable to an increase in the number and efficiency of conducting pathways in the bulk of the films. © 2002 Elsevier Science B.V. All rights reserved.

Keywords: Amorphous carbon; Field emission; Emission sites; Emission mechanism

1. Introduction

There is much current interest in the electron field emission from carbon-based materials, such as diamond [1–4], diamond-like carbon (DLC) [5–7], and carbon nanotubes [8–12]. This is because such films, when used as the cathode in field emission displays (FEDs), possess many outstanding performance criteria of potential value to the flat panel display market. However, field emission from such films does not occur uniformly over the entire surface, but from isolated emission sites scattered apparently randomly across the area under test. If such films are to be used for commercial FEDs, where brightness and uniformity of display are paramount, the density of these emission sites needs to be high (typically 10⁶ sites cm⁻²) and each site needs to carry a relatively high current load. As a result, several field emission studies of these films have involved imaging the emission sites—either by utilizing a phosphor-coated screen to observe the visible emissive spots

[13–17] or by using a point probe scanner to produce a two-dimensional current emission map [7,18]. Quantitative values for the site density have also been reported following surface caesiation [12] and etching [13]. However, these emission site densities were measured at high electric fields, with correspondingly high emission currents, where the emission characteristics may not necessarily mirror those displayed at lower applied fields.

The effects of annealing on the field emission efficiency are still not understood. Modifications of the defect distribution in, and microstructure of, hydrogenated amorphous carbon (a-C:H) films induced by vacuum annealing at high temperature have been attributed to hydrogen loss and also to graphitization [19]. However, previous work on low-temperature thermal-annealing of nitrogen-containing hydrogenated amorphous carbon (a-C:H:N) films [20] indicated that structural modification of the film is probably important, and recent studies [21] of hydrogen-free amorphous carbon (a-C) films suggest that thermally-induced structural modification is physical (e.g. surface/sub-surface mod-

*Corresponding author.

E-mail address: MT.Kuo@itri.org.tw (M.T. Kuo).

ifications) rather than chemical (e.g. graphitization) in origin. The work presented in this paper examines the emission sites closely, presents evidence concerning this issue, and reveals the effect of annealing on the site density in a-C films.

2. Experimental

a-C films were deposited in a conventional 13.56 MHz radio frequency capacitively-coupled parallel-plate reactor. The films were deposited simultaneously at a temperature of 25–60 °C, onto two lightly boron-doped Si(100) substrates (4×4 cm), using a CH₄ flow rate of 10 sccm at a DC bias of –300 V and a chamber pressure of 20 mtorr for 30 min. Micro-combustion analysis showed the films to contain <1% hydrogen and no other impurities, and so can be considered as virtually H-free amorphous carbon films. One of the samples was annealed in vacuum ($\leq 1 \times 10^{-5}$ torr) at 200 °C for 48 h. The temperature of 200 °C was chosen based on the results of previous annealing experiments [20,21] that showed that temperatures below this had no significant effect upon film characteristics, but at higher temperatures the films tended to evaporate off. The thickness of the films was measured by cross-sectional scanning electron microscopy (SEM) and found to have a uniformity over the 1 cm² sample area of about $\pm 5\%$. The film thickness of the as-deposited film and the annealed film were 640 nm and 460 nm, respectively, showing that annealing has caused film shrinkage, although there was no evidence of changes to the surface morphology or flatness.

Emission measurements were performed using a parallel plate configuration in a vacuum chamber at 3×10^{-7} torr. The anode was indium tin oxide (ITO) coated glass (2.5×2.5 cm), which had a thin layer of P22G (ZnS:Cu:Al) phosphor (2 cm in diameter) covering the center of the ITO film. The overall emission current collected by the entire ITO film was scaled by the collection area to obtain the actual current density on the phosphor. SEM analysis showed that no electron impact damage to the phosphor screen was observed for electric fields up to ~ 25 V μm^{-1} , and also that no damage to the anode surface had occurred as a result of sputtering or arc discharges (at least for the resolution possible with SEM). The anode-to-film spacing of 100 μm was maintained by polytetrafluoroethylene (PTFE) spacers. The locations of anode and spacers over the sample were adjusted carefully to avoid unwanted emission from the sample edges. It is possible that asperities in the film or the anode can be the origin of emission sites. However, our films and anode were smooth (the roughnesses are within several and tens of nm, respectively). Also, precautions were taken to avoid creation of asperities during testing, such as small ramping voltage steps and limiting the maximum applied voltage

(25 V μm^{-1}). Also, during testing, the emission sites were observed to check that unusual emission features, which may be due to asperities, did not appear. Furthermore, shorts from asperities and edges should show a linear relationship between current and voltage. Since this linear dependence was not observed, we are confident that the emission was from true emission sites, not asperities. A camcorder was focused onto the phosphor and used to record observations in real-time as the field was altered.

A conditioning process was required to initiate stable emission from the as-deposited film. This process consisted of ramping the applied voltage in 5 V steps until emission was observed. This was repeated for 3–10 cycles until the emission characteristics became repeatable. Such a conditioning process was not necessary for the annealed film, however. In order to prevent the accidental breakdown of films or damage to the phosphor screen from high energy electrons, the maximum electric field and the ramping rate were limited to 25 V μm^{-1} and 5 V per step, respectively. For the annealed and as-deposited films, the threshold fields (required to produce a measured current density of 1 $\mu\text{A cm}^{-2}$) were 4.5 and 7.2 V μm^{-1} , respectively.

3. Results and discussion

During field emission testing, the emission current was observed to increase with applied voltage in a step-wise fashion. Each jump in current was seen to coincide with the appearance of a new emissive spot on the phosphor screen. To understand the relationship between emission sites and emission current, the individual emissive spots visible on the phosphor screen were counted. Fig. 1 shows images of the phosphor screen revealing the spatial distribution of emission spots across the film surface, for both the as-grown and annealed a-C films, at three different applied fields. Clearly, the annealed film shows a much better uniformity of emission sites.

We recognize that the true number of emission sites could be larger than the number of observed emissive spots, since the latter depends on the energy of the emitted electrons being sufficient to activate the phosphor. However, the chosen high efficiency low voltage phosphor is well suited to displaying emissive spots excited by low-energy electrons emitted at or near the threshold field. Thus, we expect that, at low electric fields, the observed number of emissive spots provide a good estimate of the number of actual emission sites.

Individual emission sites are by no means stable with time, and the brightness of the sites, and hence the emission current varied quite considerably. Fig. 2 gives an indication of the observed dynamic behavior of the emission spots with time, for a constant applied field. As time progressed, new sites were observed to turn on, some existing ones turned off, while others fluctuated

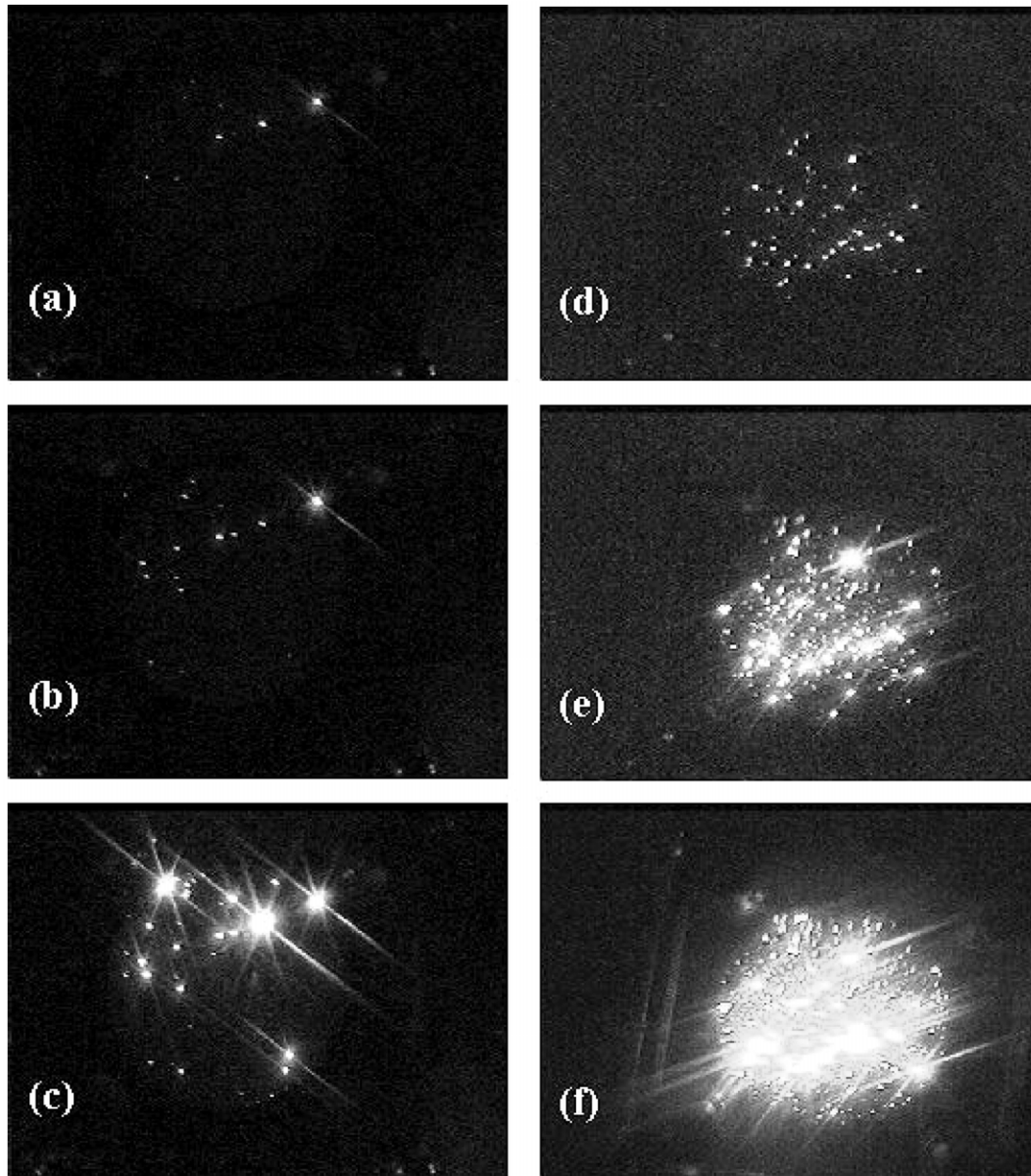


Fig. 1. Images of emission spots on the phosphor screen for as-deposited (a)–(c) and annealed (d)–(f) films at $E=9, 11$ and $15 \text{ V } \mu\text{m}^{-1}$, respectively. The photographs are one frame of a video captured from the analogue output of a camcorder.

in brightness. Emission sites were seen to turn on again even after they had turned off earlier. It was often observed that as one site died, another one appeared to replace it. New emission sites seemed to be created preferentially close to existing sites, especially where the existing site was bright. This indicated a possible self-leveling mechanism, whereby sites with too much current density create new nearby sites to share some of their current load. This may be another aspect of the ‘conditioning’ steps required to obtain reliable emission.

Fig. 3 shows that, for both films, the observed number of emissive spots (N) is proportional to the applied field, E , at least in the E range where N is countable, although we note in passing that plots of N vs. E^2 show

comparable correlation coefficients. The slopes of the $N-E$ plots for the two films are very different, however, with the annealed film showing an eight-fold steeper gradient than the as-deposited film. This implies that, compared with the as-deposited film, the emission sites in the annealed film turn on much more uniformly. As E is increased, however, precise counting of the emission spots becomes impractical, and some of the emission spots became large and very bright (see, for example, Fig. 1c,f). The large, bright spots reflect those sites that make a dominant contribution to the overall emission current. Such high current densities in a small number of sites can lead to problems with current limitation and space-charge effects, as noted by Hart et al. [13].

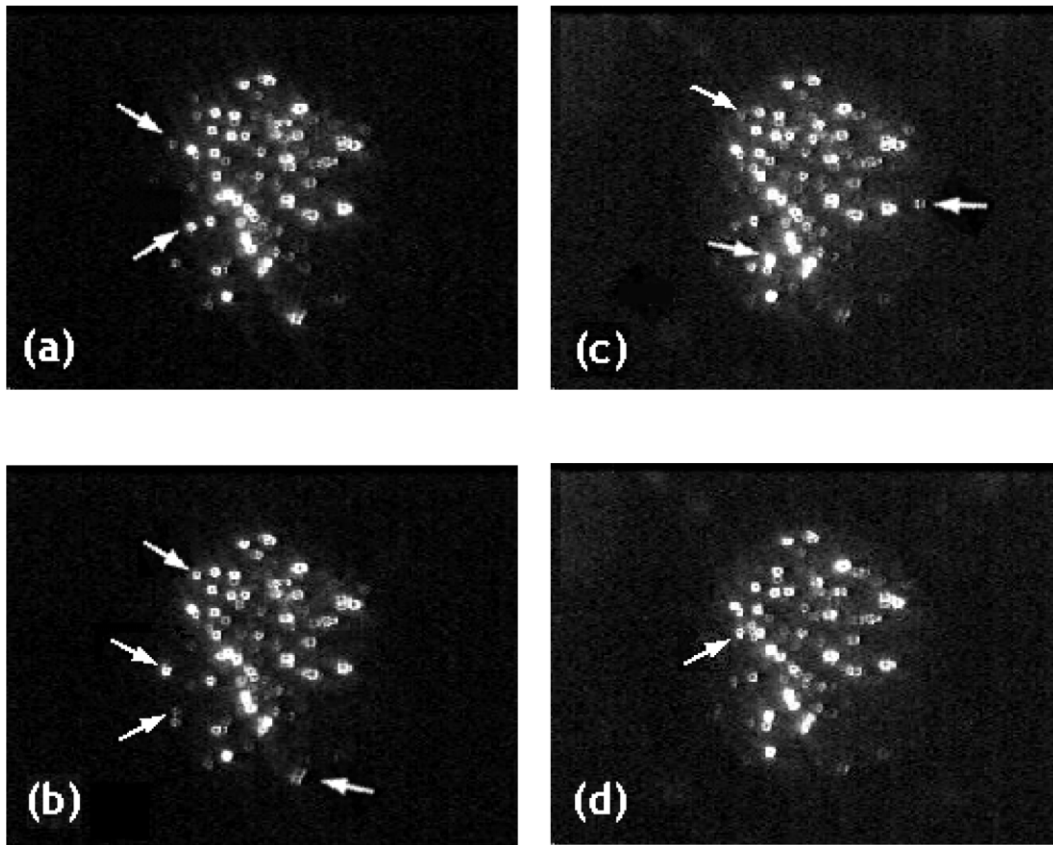


Fig. 2. Images of emission spots on the phosphor screen for an annealed a-C film at $E = 10 \text{ V } \mu\text{m}^{-1}$ taken after different durations of continuous emission. Again, the images are single-frame snapshots from a continuous video. The pictures show emission sites turning on and off, with the emission current fluctuating accordingly between a maximum of 500 and a minimum of 300 nA. (a) At the start of emission (0 min). The arrows show emission spots that are initially bright, but which fade and then turn off. (b) After 10 min. The three left-hand arrows point to new emission spots which have turned on, while the arrow on the right of the picture shows an emission spot beginning to fade. (c) After 20 min. The two lower arrows point to new spots which have turned on, while the upper arrow shows that the spot which turned on earlier in (b) is now fading. (d) After 30 min. Another new spot has appeared (indicated by the arrow), but the fading spot identified in (c) has now turned off.

Fig. 3 also demonstrates that, although N scales linearly with E , the corresponding emission current (I) rises nearly exponentially with E . The emission site density (D) and the current density (J) can be obtained simply by dividing N and I , respectively, by the area (A) of the phosphor screen. Emission site densities at higher E may be estimated by extrapolating the linear trend-line in Fig. 3, though we recognize that such a procedure has its limitations since, at higher E , a subset of the sites appear to make a disproportionate contribution to the overall current and space-charge effects are to be expected. To explore further the electron emission characteristics of these films we sought relationships between N and I (or D and J). Fig. 4 shows that, at least at low N , there is a particularly good correlation between N and $\ln(I)$, as given by Eq. (1):

$$N = S \ln(I) - R \quad (1)$$

with gradient S and intercept R . Figs. 3 and 4 provide further illustration of the markedly superior electron emission characteristics of the annealed film (both in

terms of the total emission current and the number of contributing emission sites at any given E).

Electron emission into vacuum is often considered in terms of the simplified Fowler–Nordheim equation [22], which can be written:

$$I = k\phi^{-1}(\beta V)^2 \exp(-c\phi^{3/2}/\beta V) \quad (2)$$

where β is the geometrical enhancement factor, ϕ the potential barrier to electron emission, and c and k are numerical constants. The applicability of such a model is usually tested by plotting $\ln(I/V^2)$ vs. $1/V$ which, as Fig. 5 shows, provides a reasonable straight line for both the as-deposited and post-annealed films. Eq. (2) might encourage interpretation of the shallower slope of the Fowler–Nordheim plot for the annealed film in terms of a reduction in the effective ϕ or an enhancement of β . Clearly, such a global interpretation is questionable given the obvious ‘stepwise’ nature of the electron emissions that contribute to the measured I . Indeed, at least at low fields where N is directly measurable, we also find a good correlation between N

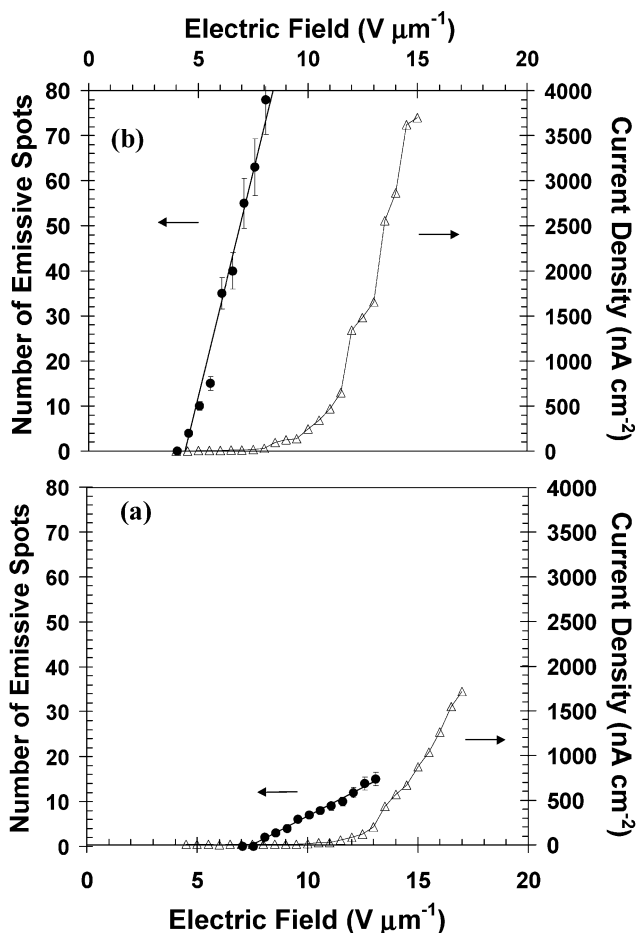


Fig. 3. Plots showing variations of the number of observed emission sites, N , (shown as \bullet) and the emission current density, J , (shown as Δ) with E , for (a) as-deposited and (b) annealed a-C films.

and $\ln(I/V^2)$, and between $\ln(N)$ and $1/V$, with the correlation coefficient $r^2 > 0.98$ for both films. However, since N , V and I are all inter-related, we can find no obvious physical basis for these correlations.

Given N and I at any given E , the average electron emission per active site (in nA site^{-1}) can be determined. This quantity, which we term the ‘emission site conductance’, can be viewed as the average current passed by an emission site at that E . Smaller values imply more uniform emission with the current load spread over more sites. In the present case, the emission site conductance for as-deposited and annealed films at $E = 8 \text{ V } \mu\text{m}^{-1}$ is ~ 10 and $\sim 1.6 \text{ nA site}^{-1}$, respectively, i.e. thermal annealing has reduced the emission site conductance roughly six-fold. At $E = 15 \text{ V } \mu\text{m}^{-1}$, the calculated site density for the as-deposited and annealed films is ~ 8 and $\sim 105 \text{ sites cm}^{-2}$, respectively, the measured current densities are ~ 0.8 and $\sim 3.7 \text{ } \mu\text{A cm}^{-2}$ (which in the case of the annealed film, at least, appears to be distributed uniformly over the entire cathode area—see Fig. 1f) and the deduced emission

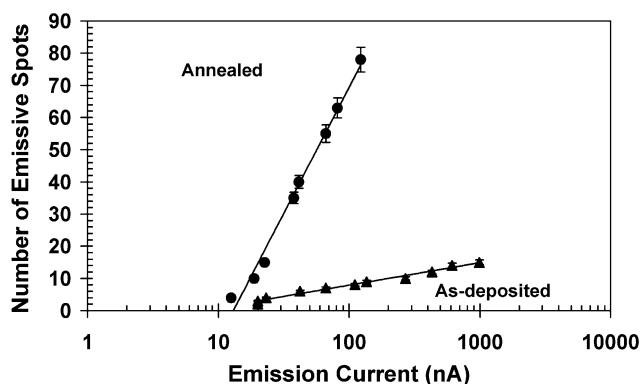


Fig. 4. Number of observed emissive spots as a function of the emission current, I , plotted on a logarithmic scale, for as-deposited (\blacktriangle) and annealed a-C (\bullet) films. Fits the data in terms of Eq. (1) yield $S = 2.6$, $R = 16.7$ and $S = 20.1$, $R = 87.5$ for the as-deposited and annealed films, respectively.

site conductances have risen to 100 and 35 nA site^{-1} , respectively.

The size and the brightness of emissive spots on the phosphor screen depend on the number and the kinetic energies of the impacting electrons. The former is presumably affected by the conducting pathways in the film while, in a Fowler–Nordheim field emission picture, the latter would be influenced by the effective work function, field enhancement factor, and interface barriers. The turn-on sequence of the observed emissions would thus presumably reflect differences in the local work function and/or the field enhancement factor for the various emission sites. A significant modification of ϕ seems unlikely, since we observe no obvious changes in optical bandgap or in the form of the Raman G-band upon annealing the a-C film (although we do note that Raman may not be sensitive enough to changes in the small volume of the sample that is occupied by emission

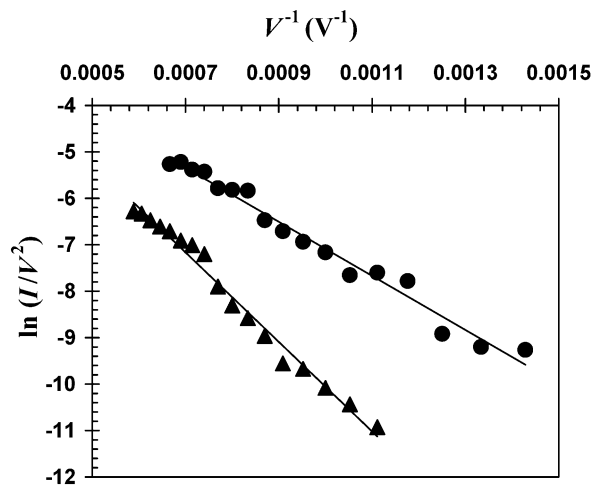


Fig. 5. Fowler–Nordheim plots of $\ln(I/V^2)$ against V^{-1} for (\blacktriangle) as-deposited and (\bullet) annealed a-C films.

sites). Thus, we attribute the improved emission characteristics of the annealed film to an enhancement of β as a result of surface and sub-surface changes that occurred when gases evolved through the surface region and, possibly, surface and sub-surface modifications induced by the so-called ‘skin effect’ [20].

The N – E plots shown in Fig. 3 reveal a much greater rate of increase in the number of emission sites for the annealed film. Previous studies of a-C:H:N films in our group [20] showed annealing to lead to an increase in the gradient of the so-called ‘first stage emission’, defined as the initial sharp onset of emission and rapid increase in I apparent in I – V plots. The emission site results presented here suggest that this increase in the gradient of first stage emission is a consequence of the improved emission site density and turn-on uniformity that accompanies annealing.

The emission site conductance results indicate that, at any given E , the emission sites on the annealed film had a smaller distributed current per site, consistent with the observation of smaller emissive spots on the phosphor screen. This might be explicable if thermal annealing enables diffusion of atoms between the substrate and film, thereby relieving internal stress in the bulk and at the interface [23–25]. However, such diffusion is not generally presumed to occur at the low annealing temperatures used in the present work [26]. Alternative explanations include: (a) the emission sites have large field enhancement factors; or (b) annealing enhances the formation of efficient bulk conducting channels that route electrons toward the observed emission sites. Mechanism (a) seems possible due to the creation of surface/sub-surface modifications (i.e. craters on the film surface created by evolved gases) as mentioned earlier. Mechanism (b) provides another plausible explanation, and we conclude by speculating how annealing might improve the conducting pathways within these films, so leading to improved field emission.

As-grown carbon-based films can be viewed as nanostructured, electrically heterogeneous materials consisting of small conducting inclusions in a dielectric matrix [27]. The conducting inclusions are generally considered to act as the media for electron transport [28–30]. Thermal annealing in vacuum, even at low temperatures, can induce several changes in the electrical properties of the film. It can cause diffusion of embedded stable molecules, from the bulk into the vacuum, thereby promoting graphitization of the remaining film and improving bulk conductivity (since more conducting clusters can be formed). Such is expected to be of limited importance in the present study since the deposited films have <1% hydrogen incorporation and so can be considered essentially pure carbon. Nevertheless, any electrically inactive inclusions embedded within the film can be expected to impede electron transport in the bulk. Further annealing can lead to graphitization and

film shrinkage. Larger and more well-ordered graphitic clusters may form, which would tend to reduce electron hopping distances and the resistance to conduction. Consistent with such a model, our earlier studies of N and P-doped DLC films [20,31,32] showed the measured field emission threshold to scale with film thickness. In the present case, however, laser Raman spectroscopy reveals no obvious graphitization of the annealed a-C film [21]. To explain the present observations we thus suppose that annealing encourages rearrangement of the nanostructure of the film—consistent with the observed film shrinkage, thereby reducing both the pore size (the ‘skin effect’) and resistance to electron transport in the bulk, and enhancing the number of ‘active’ conduction channels (thereby accounting for the greatly enhanced uniformity of observed emission sites in the annealed film).

4. Conclusions

Electron emission from as-grown and annealed a-C films has been monitored using a phosphor- and ITO-coated glass plate to allow simultaneous measurement of both the total emission current, and its spatial distribution, as a function of applied field, E . For both films, increasing E leads to a linear increase in N , the number of emission sites, but an exponential increase in the emission current, I . Thermal annealing of the a-C film enhances the electron emission at any given E , and the emission site density and uniformity. As a result, the average emission current per site [which we term the ‘emission site conductance’ (units nA site⁻¹)] is actually considerably reduced in the case of the annealed a-C film, which yields current densities $>3 \mu\text{A cm}^{-2}$ at $E=15 \text{ V } \mu\text{m}^{-1}$. The improved performance induced by annealing is most likely due to increases in the number of conducting pathways in the film bulk caused by compaction of the film.

Acknowledgments

The authors are grateful to Dr M. Waite of Brimar Ltd. for providing the efficient phosphor screens used in this work, and to K.N. Rosser for his help and interest in the project.

References

- [1] M.W. Geis, J.C. Twichell, *Appl. Phys. Lett.* 67 (1995) 1328.
- [2] O. Gröning, O.M. Küttel, E. Schaller, P. Gröning, L. Schlappbach, *Appl. Phys. Lett.* 69 (1996) 476.
- [3] M.W. Geis, J.C. Twichell, N.N. Efremow, K. Krohn, T.M. Lyszczarz, *Appl. Phys. Lett.* 68 (1996) 2294.
- [4] W.N. Wang, N.A. Fox, T.J. Davis, J.W. Steeds, in: P. Ito (Ed.), *Recent Progress in Diamond Electronics*, World Scientific, Tokyo, 1998, p. 189.
- [5] B.S. Satyanaryana, A. Hart, W.I. Milne, J. Robertson, *Appl. Phys. Lett.* 71 (1997) 1431.

- [6] G.A.J. Amaratunga, S.R.P. Silva, *Appl. Phys. Lett.* 68 (1996) 2529.
- [7] A.A. Talin, T.E. Felner, T.A. Friedmann, J.P. Sullivan, M.P. Siegal, *J. Vac. Sci. Technol. A* 14 (1996) 1719.
- [8] J.M. Bonard, J.P. Salvetat, T. Stockli, W.A. de Heer, L. Forro, A. Chatelain, *Appl. Phys. Lett.* 73 (1998) 918.
- [9] Q.H. Wang, T.D. Corrigan, J.Y. Dai, R.P.H. Chang, *Appl. Phys. Lett.* 70 (1997) 3308.
- [10] A.N. Obraztsov, A.P. Vokov, I. Pavlovsky, *Diamond Relat. Mater.* 9 (2000) 1190.
- [11] W.B. Choi, D.S. Chung, S.H. Park and J.M. Kim, *SID 99 DIGEST*, 1134 (1999).
- [12] J.M. Kim, W.B. Choi, N.S. Lee, J.E. Jung, *Diamond Relat. Mater.* 9 (2000) 1184.
- [13] A. Hart, B.S. Satyanaryana, W.I. Milne, J. Robertson, *Appl. Phys. Lett.* 74 (1999) 1594.
- [14] G.A.J. Amaratunga, M. Baxendale, N. Rupasinghe, et al., *New Diamond Frontier Carbon Technol.* 9 (1999) 31.
- [15] B.L. Ward, O.-H. Nam, J.D. Hartman, et al., *J. Appl. Phys.* 84 (1998) 5238.
- [16] R.J. Nemanich, P.K. Baumann, M.C. Benjamin, et al., *Appl. Surf. Sci.* 130-132 (1998) 694.
- [17] D.S. Mao, J. Zhao, W. Li, et al., *Diamond Relat. Mater.* 8 (1999) 52.
- [18] L.S. Pan, T.E. Felner, D.A.A. Ohlberg, W.L. Hsu, C.A. Fox, R. Cao, G. Vergara, *J. Appl. Phys.* 82 (1997) 2624.
- [19] J.K. Walters, D.M. Fox, T.M. Burke, O.D. Weedon, R.J. Newport, W.S. Howells, *J. Chem. Phys.* 101 (1994) 4288.
- [20] M.T. Kuo, P.W. May, M.N.R. Ashfold, *Diamond Relat. Mater.* 10 (2001) 889.
- [21] M.T. Kuo, PhD Thesis, University of Bristol, UK, 2001.
- [22] S.R.P. Silva, G.A.J. Amaratunga, J.R. Barnes, *Appl. Phys. Lett.* 71 (1997) 1477, References therein.
- [23] P.C. Kelires, *Int. J. Mod. Phys. B* 14 (2000) 256.
- [24] A.C. Ferrari, B. Kleinsorga, N.A. Morrison, A. Hart, V. Stolojan, J. Robertson, *J. Appl. Phys.* 75 (1999) 7191.
- [25] R. Kalish, Y. Lifshitz, K. Nugent, S. Praver, *Appl. Phys. Lett.* 74 (1999) 2936.
- [26] J. Huang, L. Wang, J. Wen, Y. Wang, C. Lin, M. Östling, *Diamond Relat. Mater.* 8 (1999) 620.
- [27] R.G. Forbes, *Solid State Electronics* 45 (2001) 779.
- [28] B.R. Chalamala, R.M. Wallace, B.E. Gnade, *J. Vac. Sci. Technol. B* 16 (1998) 2866.
- [29] Y.K. Yap, S. Kida, Y. Wada, M. Yoshimura, Y. Mori, T. Sasaki, *Diamond Relat. Mater.* 9 (2000) 1228.
- [30] V.V. Zhirnov, J. Liu, G.J. Wojak, J.J. Cuomo, J.J. Hren, *J. Vac. Sci. Technol. B* 16 (1998) 1188.
- [31] M.T. Kuo, P.W. May, A. Gunn, J.C. Marshall, M.N.R. Ashfold, K.N. Rosser, *Int. J. Mod. Phys. B* 14 (2000) 295.
- [32] M.T. Kuo, P.W. May, M.N.R. Ashfold, *Diamond Relat. Mater.* 9 (2000) 1222.